

Successful growth of low carrier density α -In₂Se₃ single crystals using Se-flux in a modified Bridgman furnace

Soumi Mondal¹, Sreekant Anil², Saurav Islam¹, Yingdong Guan¹, Sai Venkata Gayathri Ayyagari², Aaron Pearre¹, Sandra Santhosh¹, Nasim Alem², Nitin Samarth¹, Zhiqiang Mao^{1,2a)}

¹Department of Physics, The Pennsylvania State University, University Park, Pennsylvania 16802, USA

²Department of Materials Science and Engineering, The Pennsylvania State University, University Park, PA 16802, USA

Abstract

Indium selenide (In₂Se₃) has garnered significant attention for its intriguing properties and applications in batteries, solar cells, photodetectors and ferroelectric devices. However, the controlled synthesis of single phase α -In₂Se₃ remains challenging owing to its complex phase diagram, presence of multiple polymorphs and the high volatility of selenium that induces non-stoichiometry and unintentional carrier doping. For ferroelectric α -In₂Se₃, minimizing the carrier density is essential because leakage current can obscure polarization switching. Here, we report the growth of α -In₂Se₃ single crystals using a unique approach, the Se-flux assisted modified vertical Bridgman technique combined with liquid encapsulation under high pressure. This approach creates a high-pressure, Se-rich environment that effectively minimizes Se-vaporization. Structural and compositional analysis using X-ray diffraction, transmission electron microscopy and energy-dispersive X-ray spectroscopy confirm the formation of pure α -In₂Se₃ single crystals with 3R stacking. Furthermore, the crystals exhibit remarkably low carrier density of 1.5- 3.2×10^{16} cm⁻³ at 300K—the lowest reported to date, reflecting a significant suppression of Se-vacancies relative to the conventional Bridgman or melt-grown crystals. Through transport and ARPES measurements on different batches of crystals, we also demonstrate that the amount of Se-flux plays a crucial role in controlling Se-vacancies. Our results thus establish this modified Bridgman method as an effective strategy for synthesizing large α -In₂Se₃ single crystals with reduced intrinsic defects. This technique can be broadly applied to grow other volatile chalcogenides with reduced defects and controlled stoichiometry.

^{a)} Author to whom correspondence should be addressed: zim1@psu.edu

Introduction

Indium selenide (In_2Se_3) has emerged as a technologically important material owing to its remarkable electrical, optical as well as thermoelectric properties and potential applications in ionic batteries, solar cells, photodiodes, phase-change memory and other optoelectronic devices ^{1–8}. Among its polymorphs, the α – In_2Se_3 has attracted particular attention, due to the observation of room-temperature ferroelectricity in the ultrathin flakes^{9–15}. More recently, α – In_2Se_3 has been found to exhibit bulk photovoltaic effect (BPVE) and photo-ferroelectric response, further extending its potential for next generation energy-efficient photodetectors and terahertz (THz) applications^{16–18}.

Despite its promise, controlled synthesis of α – In_2Se_3 remains non-trivial. In_2Se_3 exhibits rich polymorphism – α , β , γ , δ phases with temperature-dependent phase transitions ($\alpha \rightarrow \beta$ at $\sim 200^\circ\text{C}$, $\beta \rightarrow \gamma \rightarrow \delta$ at higher temperatures, as shown in **Fig. 1b**) frequently resulting in mixed-phase crystals^{19–24}. Moreover, the α – In_2Se_3 itself comprises two stacking variants – 2H (P6₃mc) and 3R (R3m)^{19,20}, often coexisting in one sample¹³. The complexity of In-Se phase diagram, which includes other stable stoichiometries such as InSe , In_4Se_3 , and In_6Se_7 ²³, along with selenium's high vapor pressure that induces Se loss and vacancies, further complicates the growth. As a result, the In_2Se_3 crystals grown using conventional methods such as Bridgman or melt growth often exhibit phase mixing and high defect densities^{13,19–22,24,25}. Although ferroelectricity in α – In_2Se_3 has been inferred from piezoresponse force microscopy (PFM) on thin-flakes and tunnel junctions, reliable polarization-electric field (P-E) loops measurements remain elusive due to leakage current arising from typically high carrier concentrations.

Until now, several approaches have been explored to synthesize α – In_2Se_3 single crystals, including melt growth^{19,21,22,26}, chemical vapor transport (CVT)^{8,19,27} and, most commonly, the Bridgman and temperature-gradient methods^{28–33}. However, CVT and Bridgman grown crystals typically exhibit high room temperature electron densities in the range of $5 \times 10^{17} – 2 \times 10^{18} \text{ cm}^{-3}$ ^{29–32}, indicating a significant concentration of Se vacancies, which limits the material's electronic and ferroelectric performance. Although long-term post-growth annealing was reported to be effective in reducing the carrier density down to $3–7 \times 10^{16} \text{ cm}^{-3}$ at 300K^{24,26,34–36}, these studies

were performed on polycrystals or “almost single crystals” and lacked proper structural characterization, implying those reported low carrier density may not be intrinsic. These challenges highlight the need for single-phase α – In_2Se_3 single crystals with controlled stoichiometry and significantly reduced carrier density, without compromising the crystalline quality or phase purity. More recently, high pressure and high temperature (HPHT) method³⁷ and growth from saturated solutions in Se vapor³⁸ have been reported to achieve controlled growth of α – In_2Se_3 . However, the carrier density was not reported for those samples.

In this work, we introduce a unique crystal growth method, the Se-flux assisted modified vertical Bridgman method to grow pure α – In_2Se_3 single crystals. This modified Bridgman furnace uses a double-crucible geometry as shown in **Fig. 1a**, enabling continuous feeding of source material from the upper crucible to the lower growth crucible, and hence also called double crucible vertical Bridgman (DCVB). In addition, it supports liquid encapsulation and high-pressure growth, both of which are advantageous for volatile chalcogenide growth as it can suppress vaporization of the volatile element. Our group has previously demonstrated the successful synthesis of high quality Bi_2Se_3 single crystals with reduced defect using this novel method³⁹.

Although the Bridgman growth of In_2Se_3 using small amounts of excess In (6 mol%)²⁹ and excess Se (2-3 mol % excess)⁴⁰ has been reported, no prior work utilized the Se-flux environment to grow In_2Se_3 single crystals so far. The In-Se phase diagram (**Fig. 1b**) indicates that stoichiometric In_2Se_3 crystals can probably be grown from melts containing highly excessive Se near the eutectic concentration, though using significant Se exceeding the eutectic concentration will drive the formation of In_2Se_3 –Se mixture. Motivated by this idea, we attempted Se-flux growth with a significant Se-flux of 20% and 29.3% excessive relative to stoichiometric Se, marked by two red dashed lines below the eutectic point in **Fig. 1b**. To prevent this excess Se from vaporizing, boron oxide (B_2O_3) was chosen as the liquid encapsulant. Due to its chemical inertness, low density and relatively low melting point ($\sim 450^\circ\text{C}$) than the III-VI semiconductor, B_2O_3 forms a protective liquid layer over the melt, effectively minimizing the vaporization of Se under high pressure. Although the continuous feeding mode could not be utilized for In_2Se_3 growth due to its high volatility, we successfully synthesized single crystals of α – In_2Se_3 with significantly reduced Se vacancies using this modified Bridgman technique.

Structural and compositional characterization from X-ray diffraction (XRD), transmission electron microscopy (TEM) and energy-dispersive X-ray spectroscopy (EDXS) confirm the synthesis of single-phase α – In_2Se_3 single crystal with 3R stacking. Most notably, our α – In_2Se_3 single crystals exhibit a remarkably low carrier density of $1.5 \times 10^{16} \text{ cm}^{-3}$ at 300K, which further decreases to $4 \times 10^{15} \text{ cm}^{-3}$ at 10K. To the best of our knowledge, these values represent the lowest carrier densities for α – In_2Se_3 single crystals reported to date and are 1-2 order of magnitudes lower than the crystals grown by conventional Bridgman methods ($5 \times 10^{17} – 2 \times 10^{18} \text{ cm}^{-3}$ at 300K)^{29–32}. This substantial reduction in carrier density correlates with the reduction in Se vacancies achieved by using Se-flux during the growth. These results establish the Se-flux-assisted modified Bridgman method, combined with liquid encapsulation under high pressure, as a promising pathway for growing large, single-phase α – In_2Se_3 single crystals with much lower defect concentration.

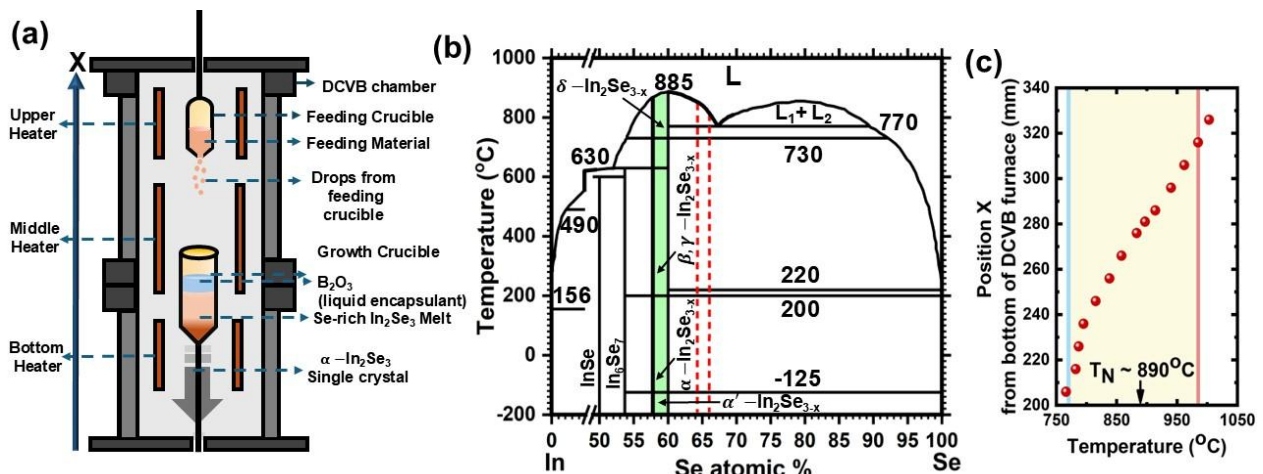


Figure 1. (a) Schematic of modified Bridgman Furnace with double-crucible geometry. (b) Schematic of the In-Se phase diagram obtained from previous reports^{23,41,42}. The green region corresponds $\text{In}_2\text{Se}_{3-x}$ (In_2Se_3 with Se vacancies) and the two red dashed lines indicate the Se concentrations used for growing In_2Se_3 . (c) The temperature profile used for the growth of In_2Se_3 crystal. The start and the end temperatures of the translation are marked by the red and blue lines respectively, while the yellow background shows the entire temperature range over which the crystal growth occurred. T_N refers to the melting point of In_2Se_3 .

Methods

α – In_2Se_3 crystals were grown by employing a combination of Bridgman and flux-growth methods in presence of liquid encapsulation and high pressure (up to 10 atm) in a modified Bridgman furnace. Combination of liquid encapsulation and high pressure helps to suppress the vaporization of Se and allow better control of the melt composition during crystal growth. As noted above, this furnace uses the concept of

double crucible (**Fig. 1a**), where the lower growth crucible contains the source materials and the upper crucible supplies feeding materials to the growth crucible, as shown in **Fig. 1a**. In this modified technique, the crucible loaded with the source material can be directly placed inside the high-pressure chamber, without sealing in a quartz tube. A proper amount of B_2O_3 was added to the crucible, which serves as liquid encapsulation during the growth.

Initially, we attempted using the feeding crucible to continuously supply In_2Se_3 to the lower growth crucible, since this approach may enable the traveling solvent growth as demonstrated in the DCVB growth of Bi_2Se_3 ³⁹ and thus better control crystal stoichiometry. However, due to high volatile nature of In_2Se_3 , significant vaporization occurred, leading to deposition on the upper walls and sides of the chamber instead of dripping down into the growth crucible. As a result, this feeding approach proved unsuitable for In_2Se_3 . Nevertheless, by adopting a Se-flux-assisted liquid encapsulation growth strategy under high pressure – without continuous feeding – we successfully synthesized $\alpha - In_2Se_3$ single crystals. As seen from the In-Se phase diagram in **Fig. 1b**, Se-flux growth can possibly favor the growth of In_2Se_3 crystals with less Se vacancies. Thus, we chose two different Se-flux concentrations (marked by red lines in **Fig. 1b**) close to the eutectic point to perform the growth.

High-purity In and Se powders were weighed out in a glove box under an inert atmosphere in a molar ratio of 34:66 (~2:3.88) corresponding to 29.3 % excess Se, which acted as a flux (Batch-1). For Batch-2, In and Se powders were loaded in a molar ratio of 40:72 (~ 2:3.6), corresponding to 20% Se flux. These elemental powders were thoroughly mixed and loaded in a tip-shaped alumina crucible. To prevent the vaporization of Se during heating, ~1.5g of B_2O_3 was added on top of the In-Se mixture, acting as a liquid encapsulant. The alumina crucible was then carefully mounted on the bottom shaft of the furnace, serving as the growth crucible.

After mounting the growth crucible, the chamber was evacuated to a vacuum level of $\sim 10^{-4}$ torr and then filled with Ar gas up to a pressure of 10 atm. The power of the three carbon heaters of the furnace (**Fig. 1a**) was adjusted to obtain the desired temperature gradient of $\sim 25^\circ C/cm$ suitable for the growth. Using the required input power, the temperature at the initial position of the growth crucible (close to the center of the middle zone) was set to $980^\circ C$ which is above the melting point of

In_2Se_3 (890°C), while the bottom zone was maintained at 770°C, creating the desired temperature gradient. The system was held under these conditions for 24hrs to allow homogenization of the melt. After this, crystal growth was initiated by translating the growth crucible downward from the high temperature position (980°C) to the low temperature position (770°C) at a controlled rate of 0.9 – 1.0 mm/hr. The temperature profile used for this growth is presented in **Fig. 1c**. Upon completion of the translation process, the furnace was slowly cooled down to room temperature over a period of 48hrs by gradually ramping down the heater power.

After cooling, the chamber was opened and only minimal Se deposition was observed on the growth wall chamber, confirming the effectiveness of the use of B_2O_3 liquid encapsulation and high pressure in minimizing Se vaporization. Finally, the alumina crucible was carefully broken to obtain the crystal ingot. **Figure 2a** shows the image of the Batch-1 $\alpha - \text{In}_2\text{Se}_3$ crystal grown by this new method.

XRD was used to identify the phase of the grown crystals, whereas crystal composition was analyzed using EDXS. The stacking arrangement in our $\alpha - \text{In}_2\text{Se}_3$ crystal was determined by TEM. For both TEM and STEM analyses, the lamella was prepared along the zone axis $[\bar{2}110]$ using focused ion beam (FIB) techniques. Thinning for electron transparency was accomplished with a Thermo Fisher Scientific Helios 660 NanoLab Dual-Beam FIB. Aberration-corrected STEM imaging was conducted on a Thermo Fisher Scientific Titan G2 microscope operated at 300 kV. A bandpass filter was applied to the acquired ADF-STEM images using the bandpass filtering function in GATAN Digital Micrograph. Selected-area electron diffraction (SAED) patterns and TEM images were obtained using the Thermo Fisher Scientific Talos F200X microscope at an accelerating voltage of 200 kV.

The electrical transport measurements of $\alpha - \text{In}_2\text{Se}_3$ crystals were done using the four-probe method in Quantum Design Physical Property Measurement System (PPMS). Angle-resolved photoemission spectroscopy (ARPES) measurements were carried out at 300K using the 21eV Helium I α spectral line from a helium plasma lamp, isolated using a monochromator and the emitted photoelectrons were detected using Scienta-Omicron DA 30L analyzer having a spectral resolution of 6 meV. Prior to measurements, all the samples were cleaved inside the chamber at a base pressure of 5×10^{-9} mbar to obtain a pristine surface.

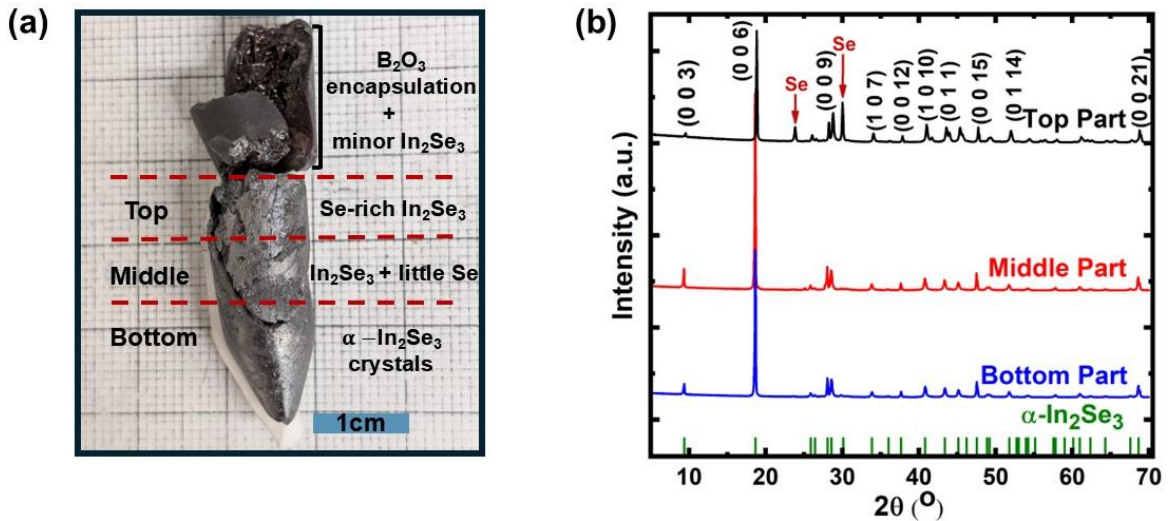


Figure 2. (a) Image of the crystal ingot grown using the DCVB Furnace without feeding (batch-1). The ingot is divided into four regions: B₂O₃ with some minor In₂Se₃, Top which corresponds to Se-rich In₂Se₃, Middle part which is In₂Se₃ with little Se and Bottom part which is pure α -In₂Se₃ single crystal. (b) Powder XRD of α -In₂Se₃ from the three different regions: Top, Middle and Bottom. Top part shows a very strong additional peak corresponding to elemental Se, which is very weak in the XRD from middle part and absent for the bottom region. Our XRD pattern matches with the simulated pattern for α -In₂Se₃ (in green) obtained from ICDD database (PDF-5+ 2026, 04-027-0925)

Characterization of the Batch-1 In₂Se₃ crystal

The top brownish layer above the grown crystal ingot (**Fig. 2a**) was identified to consist primarily of B₂O₃ with some minor incorporation of In₂Se₃, which accounts for the coloration. Minimal Se contamination was observed on the growth chamber walls which indicates that B₂O₃ served as an effective encapsulant, though with slight mixing of In₂Se₃. To investigate the composition and structural phase of the grown crystal, EDXS and XRD analysis have been performed. Based on these characterizations, the crystal is divided into three regions — Top, Middle and Bottom.

Powder XRD from the three regions of the crystal is shown in **Fig. 2b**. No secondary phases were detected in the bottom region of the crystal, and all the diffraction peaks matched with those of α -In₂Se₃, confirming the growth of pure α -In₂Se₃. In contrast, the top region exhibited an additional strong diffraction peak corresponding to elemental Se, while the middle region displayed a very weak peak of Se. These results from XRD agree with the EDXS results presented in **Fig. 3**.

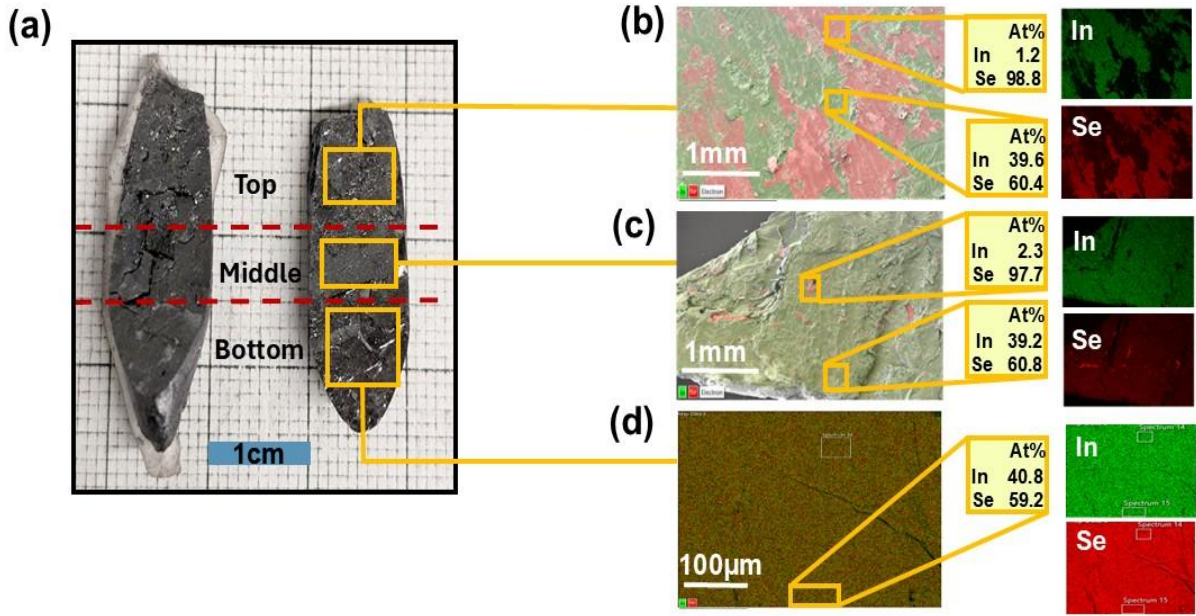


Figure 3. (a) Image of the cleaved crystals of Batch-1 α – In_2Se_3 . (b)–(d) EDXS mapping of single crystal piece cleaved from three different regions Top (b), Middle (c) and Bottom (d). Green regions correspond to In_2Se_3 and the red regions to elemental Se. The top region of the crystal has rich Se, while the middle part contains very little Se. Pure In_2Se_3 with homogenous distribution of In and Se is obtained from the bottom region of the ingot.

The top region located just below the B_2O_3 is characterized by more significant precipitates of Se, as evident from the EDXS mapping of the crystal piece cleaved from the top part (**Fig. 3b**). The green regions correspond to In_2Se_3 , and the red regions denote presence of pure Se. The middle region showed only minor Se precipitates (**Fig. 3c**), suggesting the formation of almost pure In_2Se_3 . The crystal cleaved from the bottom region reveals a homogeneous distribution of In and Se, confirming the presence of pure In_2Se_3 crystals (**Fig. 3d**). As In_2Se_3 starts to crystallize from the melt, the relative proportion of excess Se increases in the remaining melt driving the composition of the melt towards the In_2Se_3 –Se eutectic point which leads to the formation of In_2Se_3 –Se mixture in the top region.

Fig. 4a shows the image of a crystal piece cleaved from the bottom region. The single-crystalline nature of the crystal is further confirmed by the strong and prominent (00l) reflections in **Fig. 4b**. Combined XRD and EDS analyses demonstrate that the use of Se flux together with liquid encapsulation under high pressure effectively facilitates the growth of large α – In_2Se_3 single crystals.

Additionally, TEM was performed to determine whether the grown α – In_2Se_3 has 3R or 2H stacking. **Figure 4c** compares the crystal structures of 3R and 2H α – In_2Se_3 . Both the crystal structures display a van der Waals (vdW) layered framework with

each slab comprising covalently bonded Se-In-Se-In-Se quintuple layer stacked along the c-axis, while adjacent quintuple-layer slabs are coupled together by weak vdW forces. The difference between the 3R and 2H phase of α –In₂Se₃ lies in the stacking of these layers^{19,20,23,43}. The 3R α –In₂Se₃ belongs to space group R3m with rhombohedral structure characterized by three-layer periodicity where successive monolayers show a small translation along the ab plane, resulting in ABC stacking (**Fig. 4c**). In contrast, the 2H α –In₂Se₃ has a hexagonal structure with space group P6₃mc and exhibit AB stacking with two-layer periodicity (**Fig. 4c**).

A representative cross-sectional selected-area electron diffraction (SAED) pattern of our crystal (**Fig. 4d**) corresponds to the [2110] zone axis of 3R α –In₂Se₃ structure (simulated electron diffraction pattern given in **Fig. S1**, in the supplementary materials). Moreover, the atomically resolved scanning transmission electron microscopy (STEM) images presented in **Fig. 4e and 4f** reveal a clear ABC stacking sequence, further confirming the 3R polytype. However, we also observe some additional reflections in the SAED pattern acquired from slightly different region of the crystal, as shown in **Fig. S2** in supplementary material, which likely originate from twin domains.

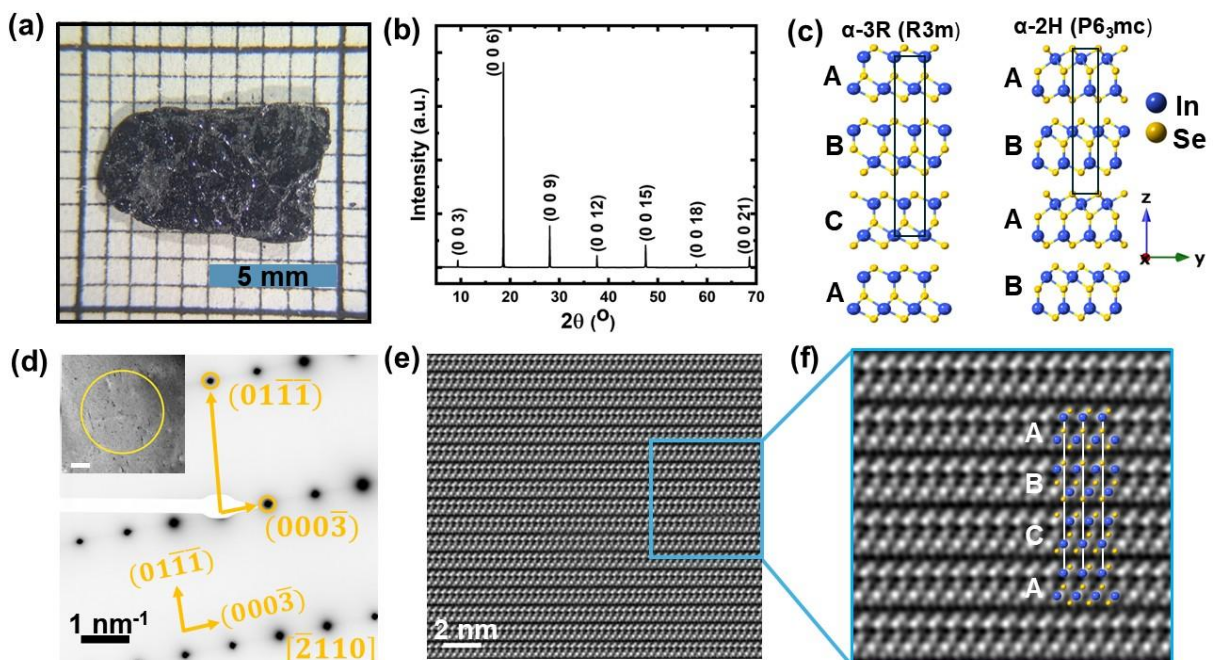


Figure 4. (a) Image of a cleaved Batch-1 crystal piece from the bottom region of the ingot. (b) XRD pattern of the crystal piece confirming the growth of α –In₂Se₃ single crystal. (c) Crystal structures of the 2H and 3R α –In₂Se₃ (d) SAED pattern of Batch-1 α –In₂Se₃ crystal along the [2110] zone with the real-space TEM image shown as inset (inset scale bar: 200nm) (e) ADF-STEM image of the crystal piece showing ABC stacking sequence, confirming 3R phase in Batch-1 α –In₂Se₃. (f) A zoomed-in region in which the atomic model of 3R α –In₂Se₃ projected along the direction [2110] is overlaid. .

Electronic property of Batch-1 α –In₂Se₃ crystal

α – In₂Se₃ can exhibit a variety of defects such as cationic vacancy V_{In}, interstitial In atoms (In_i) and anionic selenium vacancy (V_{Se})²⁵, however, undoped In₂Se₃ crystals are consistently observed to be n-type reflecting that Se vacancies are the most dominant defects in this compound⁴⁴. Since the presence of Se vacancies act as electron donor, it is expected that reduction in the concentration of these vacancies will lower the carrier concentration (n_e), improving the crystal quality. Previous studies have reported that α –In₂Se₃ crystals, grown by Bridgman method, are electron doped with in-plane electron conductivity (σ) in range of 20-68.9 $\Omega^{-1}\text{cm}^{-1}$ and carrier density ranging from 5×10^{17} – 2×10^{18} cm^{-3} at 300K^{29–32}. The α –In₂Se₃ single crystal grown with indium excess exhibited metallic like behavior with σ and n_e increasing with decrease in temperature²⁹.

The influence of post-growth annealing on the electrical properties of α –In₂Se₃ was investigated several years ago as mentioned earlier^{24,34,35}. Crystals synthesized by direct fusion of elements and subsequently subjected to prolonged annealing and slow cooling exhibited lower electron density of approximately $3-7\times10^{16}$ cm^{-3} , accompanied by low in-plane conductivity $\sigma_{\text{in-plane}} \sim 0.1 \Omega^{-1}\text{cm}^{-1}$ at 300K whereas crystals quenched in liquid nitrogen showed higher electron densities of $1.4-2\times10^{19}$ cm^{-3} and $\sigma_{\text{in-plane}}$ of around $260 \Omega^{-1}\text{cm}^{-1}$ ^{24,34–36}. Furthermore, the quenched samples displayed an increasing σ upon cooling, whereas the annealed samples exhibited the opposite trend. These findings demonstrated that annealing the samples promoted defect annihilation, thereby leading to the expected decrease in the electron density. However, it is important to note that the reported measurements were performed on either polycrystalline or “almost single crystals” specimens²⁶, with no accompanying characterizations like XRD or EDXS. The absence of characterization results limits a clear assessment of the crystalline quality and defects in those samples and implies that the reported carrier density of the order of 10^{16} cm^{-3} is yet to be verified.

To assess the crystal quality of our grown α –In₂Se₃ single crystal, particularly the concentration of Se vacancies, electronic transport measurements have been carried out using a standard four-probe measurement technique. The in-plane electrical resistivity (ρ_{xx}) measured across the temperature range from 2.5K to 300K, shows an increase in ρ_{xx} value upon cooling, suggesting insulating behavior. As shown in **Fig. 5a**, the measured ρ_{xx} value is found to be 20 Ω cm at 300K, which is significantly larger than the values reported for α –In₂Se₃ Bridgman-grown crystals (0.015-0.05 Ω cm at 300K)^{28–32} and for the quenched samples (3×10^{-3} Ω cm)^{24,34–36}. This value is also larger than the resistivity obtained for annealed samples (~ 10 Ω cm)^{24,34–36}. The Hall resistivity (ρ_{xy}) versus magnetic field curves (**Fig. 5b**) exhibited a negative slope, confirming electrons as the dominant charge carriers in the sample, consistent with earlier reports.

The carrier concentration (n_e) values extracted from magnetic field-dependent Hall resistivity (ρ_{xy}) measurements at various temperatures are plotted as shown in **Fig. 5c**. At 300K, n_e was determined to be 1.5×10^{16} cm^{-3} , further dropping to a value of 4×10^{15} cm^{-3} at 10 K which is the lowest carrier density that has been reported till date for α –In₂Se₃. For comparison, the previously reported carrier densities at 25K were around 5×10^{16} cm^{-3} for the annealed samples^{34,35} and $\sim 10^{17}$ cm^{-3} for crystals grown by the conventional Bridgman method^{29–32}. Similar measurements performed on additional cleaved pieces of the same crystal also yielded n_e in the range of 1.5 – 3.2×10^{16} cm^{-3} at 300K, confirming the lowest carrier density in our grown α -In₂Se₃. These exceptionally low carrier densities, combined with high resistivity observed across multiple samples, provide strong evidence that Se-flux method produced α -In₂Se₃ single crystals with least density of Se vacancies reported so far. Despite our samples showing insulating behavior, we were unable to obtain reliable P-E hysteresis loops because of leakage currents, indicating that the crystals are still not sufficiently insulating for ferroelectric polarization measurements.

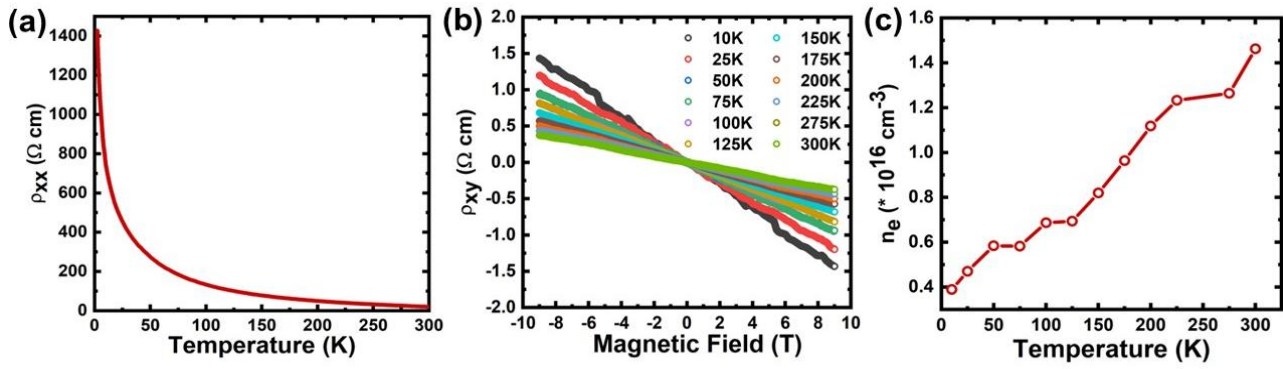


Figure 5. (a) Temperature dependent in-plane resistivity (ρ_{xx}) of α - In_2Se_3 crystal cleaved from the bottom region. (b) Magnetic field-dependent Hall resistivity (ρ_{xy}) showing negative slope, confirming electrons to be the main carriers in the DCVB grown α - In_2Se_3 . (c) Temperature dependence of Carrier density (n_e) extracted from the Hall resistivity data

Characterization and transport properties of Batch-2 In_2Se_3 crystals

The Batch-2 In_2Se_3 crystals were grown with 20% excess Se as mentioned in the methods section. The as-grown Batch-2 In_2Se_3 crystal ingot is shown in **Fig. 6a**. The ingot was divided into three regions — A, B and C for characterization similar to Batch-1 In_2Se_3 crystals. **Figure 6b** summarizes the EDXS composition analysis from all three regions. Unlike Batch-1 crystal which had a Se-rich top region, no such Se-enrichment was observed in Batch-2 crystal; instead, region A contained a mixed phase of In_2Se_3 and InSe . In contrast, the EDXS composition analysis of the crystal pieces cleaved from regions B and C confirms the formation of pure In_2Se_3 with a homogeneous composition. Furthermore, XRD scans of crystal pieces from regions B and C (**Fig. 6c**) show strong and sharp (00l) reflections confirming the growth of pure α - In_2Se_3 single crystals.

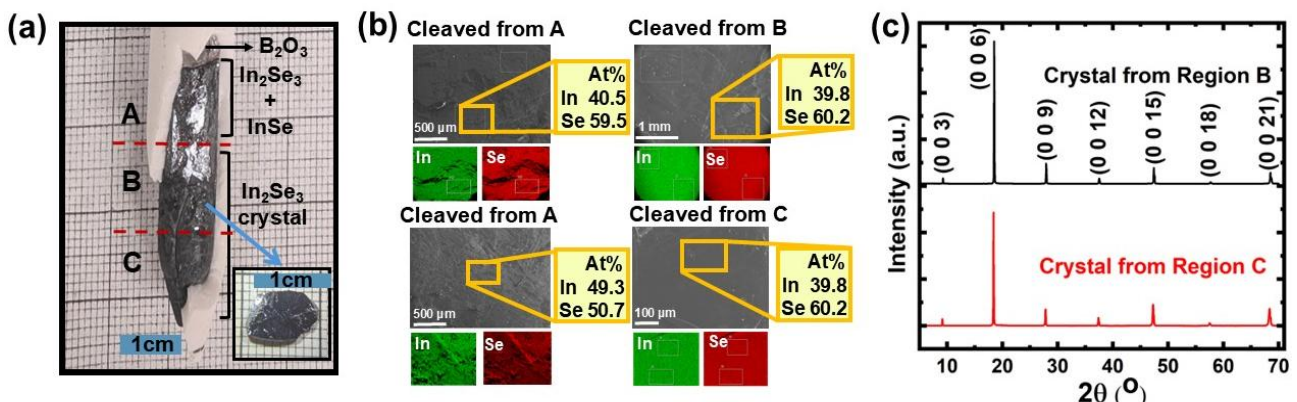


Figure 6. (a) Image of the Batch-2 In_2Se_3 crystal grown using with 20% excess selenium as flux. (b) EDXS elemental mapping and composition analysis of crystals from three different regions – A, B and C. Region A exhibits coexistence of In_2Se_3 and InSe ; whereas regions B and C show pure In_2Se_3 with a homogeneous distribution of indium and selenium. (c) XRD patterns of the crystals from regions B and C show only (00l), indicative of their single crystalline nature.

Additionally, we performed electronic transport measurements on Batch-2 α –In₂Se₃ single crystal using PPMS to assess the density of Se-vacancies. The in-plane resistivity (ρ_{xx}) at 300K is about 63 m Ω cm, which is only 0.3% of the ρ_{xx} value observed for the Batch-1 crystal (20 Ω cm) at the same temperature. **Figure 7a** shows the variation of ρ_{xx} with temperature. Batch-2 α –In₂Se₃ single crystals displayed a broad peak in ρ_{xx} , followed by a metallic behavior, unlike Batch-1 α –In₂Se₃ single crystals which showed an insulating-like behavior. The Hall resistivity (ρ_{xy}) as a function of magnetic field showed a negative slope (**Fig. 7b**), confirming n-type behavior, consistent with both previous literature reports and our Batch-1 results. The room temperature carrier density evaluated from the Hall resistivity data (**Fig. 7c**) for Batch-2 is 2.32×10^{17} cm⁻³, smaller than the values reported for crystals grown by the conventional Bridgman method (5×10^{17} – 2×10^{18} cm⁻³ at 300K)^{29–32} but nearly an order of magnitude higher than the Batch-1 sample. This increased carrier density of the Batch-2 crystal indicates a higher concentration of Se vacancies in α –In₂Se₃ single crystals from Batch-2 than Batch-1, likely arising from the use of a reduced Se-flux (10% lower than what was used for Batch-1 growth).

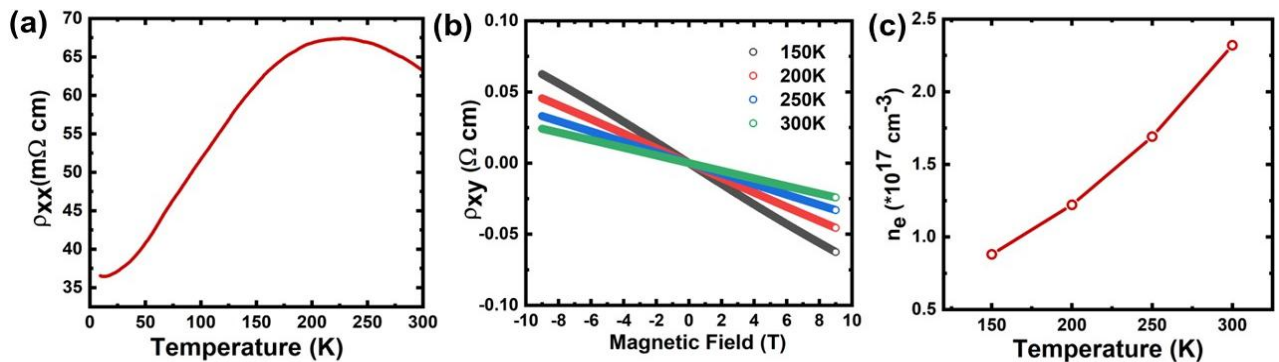


Figure 7. (a) Temperature dependence of the in-plane resistivity (ρ_{xx}) of Batch-2 α –In₂Se₃ crystal. (b) Magnetic-field dependence of the Hall resistivity (ρ_{xy}) showing negative slope, confirming electrons to be the dominant carriers in the Batch-2 grown α –In₂Se₃. (c) Temperature dependence of the carrier density (n_e) extracted from the Hall resistivity data.

Comparison between Batch-1 and Batch-2 crystals based on Angle-resolved Photoemission Spectroscopy (ARPES)

To further assess the electron doping in Batch-1 and Batch-2 α –In₂Se₃ single crystals, the electronic band structure of the bulk crystals was examined by ARPES. The ARPES spectra at 300K for two Batch-1 single crystal pieces (S1 and S2)

and one Batch-2 single crystal (S1) piece are presented in **Fig. 8 (top panel)** and the corresponding second derivatives are shown in **Fig. 8 (bottom panel)**. The Batch-2 sample exhibited a well-defined inverted parabolic valence band characteristic of a Mexican hat-like band dispersion⁴³. It is also noted that the conduction band minima and the top of the valence band maxima are located close to the center of the Brillouin zone. In contrast, both Batch-1 crystal pieces showed a smeared density of states rather than distinct clear bands, likely due to the surface roughness that remained even after cleaving. We observed no signatures of bulk conduction near the Fermi level (E_F) in one of the Batch-1 samples (**Fig. 8a and 8b**), suggesting that the sample is nearly undoped. However, The ARPES spectrum for the second Batch-1 sample (Batch1-S2) and the Batch-2 sample (Batch2-S1) showed traces of bulk conduction across E_F , revealing inhomogeneous doping⁴³, which can be attributed to Se vacancies. The E_F lies approximately 0.20 eV above the conduction band minima (CBM) for Batch1-S2 and 0.31 eV above CBM in Batch2-S1.

Furthermore, the band gap values were also estimated from the ARPES spectra. Batch1-S1 and Batch1-S2 crystals have a gap of ~1.7eV whereas Batch2-S1 shows a narrower band gap ~1eV, which is consistent with our observation of insulating behavior and reduced carrier density in Batch-1 crystal compared to Batch-2. Although the Batch1 crystal was grown with higher Se flux and exhibited reduced electron density, implying fewer Se vacancies, some crystal pieces still show bulk conduction near E_F , thereby indicating that the compositional distribution remains inhomogeneous to some extent. This inhomogeneity remains undetected by EDXS, probably because of its limited resolution. The observed compositional inhomogeneity likely originates from the use of insufficient Se-flux during the growth and can probably be solved by further increasing the Se-flux during the growth.

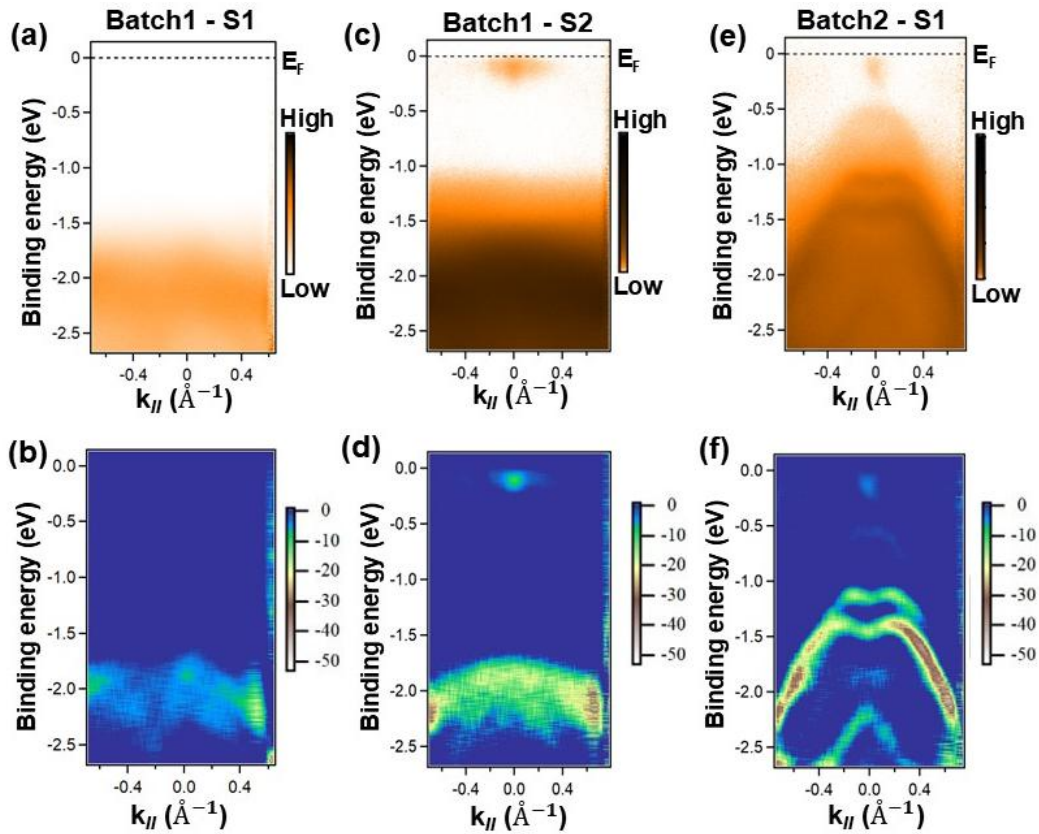


Figure 8. (a) ARPES spectra for a Batch-1 α –In₂Se₃ crystal piece (S1) at 300K. The color bar represents counts in arbitrary units. (b) The corresponding second derivative of the Batch1-S1 ARPES spectra. (c) ARPES spectra for another Batch-1 crystal piece (S2) at 300K. (d) Second derivative of the spectra shown in (c). (e) Same as (a) and (c) for a representative Batch-2 single crystal displaying an “inverted Mexican hat-like” bands. (f) Second derivative of the Batch2-S1 ARPES spectra.

Conclusion

In summary, we synthesized α –In₂Se₃ single crystals in a modified Bridgman furnace with Se-flux and liquid encapsulation under high pressure. Despite this modified Bridgman furnace having a double-crucible geometry, we could not employ the feeding method to supply source material during growth, because of high volatility of In₂Se₃. Instead, we grew two batches of In₂Se₃ using different excess Se concentrations close to the eutectic point. Structural and compositional characterization results confirmed the growth of pure α –In₂Se₃ single crystals with 3R stacking sequence. Batch-1 crystals revealed lowest carrier density reported so far ($1.5\text{--}3.2 \times 10^{16}$ cm⁻³ at 300K), about 1-2 orders of magnitudes lower than those grown using conventional methods, indicating a significant reduction in defect concentration. Though Batch-1 crystals show an overall insulating behavior, observation of bulk conduction near E_F in some pieces, together with difficulties in

getting reliable P-E loop data, suggests that the carrier density needs to be further reduced. As discussed above, this can likely be achieved by increasing Se-flux concentration during growth. In contrast, Batch-2 α – In_2Se_3 exhibited carrier density of $2.32 \times 10^{17} \text{ cm}^{-3}$ at 300K. This comparison further elucidates the critical role of Se-flux concentration in determining the stoichiometry and defect landscape of α – In_2Se_3 crystals. A higher Se-flux (29.3% excess) in Batch-1 effectively suppressed Se vacancies, resulting in a lower carrier density and more insulating behavior, whereas reducing the Se excess to 20% in Batch-2 resulted in a metallic-like behavior and a correspondingly higher carrier concentration. These results underscore the strong sensitivity of In_2Se_3 crystal growth to the Se-flux ratio used and encapsulation conditions, which are crucial for achieving near stoichiometric compositions with minimal Se vacancies.

The successful growth of In_2Se_3 further highlights the potential of this method as a promising route for growing large single crystals, particularly for metal chalcogenides with complex phase diagram and volatile constituent elements, marking a significant advancement in materials synthesis techniques.

Supplementary Material

The supplementary material contains the simulated electron diffraction patterns used to compare the electron diffraction pattern of our crystal (**Fig. S1**) and the TEM images from slightly different regions of the sample revealing some extra reflections possibly originating from the presence of twin planes (**Fig. S2**).

Acknowledgements

The crystal growth and characterization efforts were primarily supported by the U.S. Department of Energy under grant DE-SC0019068. The transport and ARPES measurements are supported the U.S. National Science Foundation (FuSe-2425599). The TEM analysis was supported by the U.S. Department of Energy under grant DE-SC0024943. S.V.G.A. and N.A. acknowledge the support from the NSF through the Pennsylvania State University Materials Research Science and Engineering Center (MRSEC) DMR-2011839 (2020-2026).

Author Declarations

Conflict of Interest

The authors have no conflicts to disclose

Author Contributions

S.M. and Y.G. carried out the crystal growth of α -In₂Se₃ under the guidance of Z.M. S.M. performed XRD and EDXS to characterize the grown crystals and performed the transport measurements. S.A., S.V.G.A and N.A. performed TEM analysis on the α -In₂Se₃ single crystals. A.P. helped to perform Laue to identify crystallographic axis for TEM measurement. S.I., S.S. and N.S. did ARPES measurements on the α -In₂Se₃ single crystals. The manuscript is prepared by S.M. and Z.M. with input from all co-authors.

Data Availability

The data that support the findings of this study are available from the corresponding author upon reasonable request.

References:

¹ J. Cui, H. Peng, Z. Song, Z. Du, Y. Chao, and G. Chen, "Significantly Enhanced Thermoelectric Performance of γ -In₂Se₃ through Lithiation via Chemical Diffusion," *Chem. Mater.* **29**(17), 7467–7474 (2017).

² H. Yuan, and Y.W. Zhang, "Role of Ferroelectric In₂Se₃ in Polysulfide Shuttling and Charging/Discharging Kinetics in Lithium/Sodium-Sulfur Batteries," *ACS Appl. Mater. Interfaces* **14**(14), 16178–16184 (2022).

³ G. Karmakar, D. Dutta Pathak, A. Tyagi, B.P. Mandal, A.P. Wadawale, and G. Kedarnath, "Molecular precursor mediated selective synthesis of phase pure cubic InSe and hexagonal In₂Se₃ nanostructures: new anode materials for Li-ion batteries," *Dalt. Trans.* **52**(20), 6700–6711 (2023).

⁴ G. Almeida, S. Dogan, G. Bertoni, C. Giannini, R. Gaspari, S. Perissinotto, R. Krahne, S. Ghosh, and L. Manna, "Colloidal Monolayer β -In₂Se₃ Nanosheets with High Photoresponsivity," *J. Am. Chem. Soc.* **139**(8), 3005–3011 (2017).

⁵ H. Lee, Y.K. Kim, D. Kim, and D.H. Kang, "Switching behavior of indium selenide-based phase-change memory cell," *IEEE Trans. Magn.* **41**(2), 1034–1036 (2005).

⁶ S. Chen, X. Liu, X. Qiao, X. Wan, K. Shehzad, X. Zhang, Y. Xu, and X. Fan, "Facile Synthesis of γ -In₂Se₃ Nanoflowers toward High Performance Self-Powered Broadband γ -In₂Se₃/Si Heterojunction Photodiode," *Small* **13**(18), 1–7 (2017).

⁷ R.B. Jacobs-gedrim, M. Shanmugam, N. Jain, and C. a Durcan, "Supporting information Extraordinary Photoresponse in Two-Dimensional In₂Se₃ Nanosheets," (1), 514–521 (2014).

⁸ Y. Hu, W. Feng, M. Dai, H. Yang, X. Chen, G. Liu, S. Zhang, and P. Hu, "Temperature-dependent growth of few layer β -InSe and α -In₂Se₃ single crystals for optoelectronic device," *Semicond. Sci. Technol.* **33**(12), (2018).

⁹ Y. Zhou, D. Wu, Y. Zhu, Y. Cho, Q. He, X. Yang, K. Herrera, Z. Chu, Y. Han, M.C. Downer, H. Peng, and K. Lai, "Out-of-Plane Piezoelectricity and Ferroelectricity in Layered α -In₂Se₃ Nanoflakes," *Nano Lett.* **17**(9), 5508–5513 (2017).

¹⁰ C. Cui, W.J. Hu, X. Yan, C. Addiego, W. Gao, Y. Wang, Z. Wang, L. Li, Y. Cheng, P. Li, X. Zhang, H.N. Alshareef, T. Wu, W. Zhu, X. Pan, and L.J. Li, "Intercorrelated In-Plane and Out-of-Plane Ferroelectricity in Ultrathin Two-Dimensional Layered Semiconductor In₂Se₃," *Nano Lett.* **18**(2), 1253–1258 (2018).

¹¹ S. Wan, Y. Li, W. Li, X. Mao, W. Zhu, and H. Zeng, "Room-temperature ferroelectricity and a switchable diode effect in two-dimensional α -In₂Se₃ thin layers," *Nanoscale* **10**(31), 14885–14892 (2018).

¹² B. Lv, Z. Yan, W. Xue, R. Yang, J. Li, W. Ci, R. Pang, P. Zhou, G. Liu, Z. Liu, W. Zhu, and X. Xu, "Layer-dependent ferroelectricity in 2H-stacked few-layer α -In₂Se₃," *Mater. Horizons* **8**(5), 1472–1480 (2021).

¹³ L. Bai, C. Ke, Z. Luo, T. Zhu, L. You, and S. Liu, "Intrinsic Ferroelectric Switching in Two-Dimensional α -In₂Se₃," *ACS Nano*, (2024).

¹⁴ J. Kim, S. Kim, and H. Yu, "Enhanced Electrical Polarization in van der Waals α -

In₂Se₃ Ferroelectric Semiconductor Field-Effect Transistors by Eliminating Surface Screening Charge," *Small* **20**(50), 1–13 (2024).

¹⁵ W. Ding, J. Zhu, Z. Wang, Y. Gao, D. Xiao, Y. Gu, Z. Zhang, and W. Zhu, "Prediction of intrinsic two-dimensional ferroelectrics in In₂Se₃ and other III₂-VI₃ van der Waals materials," *Nat. Commun.* **8**(1), 14956 (2017).

¹⁶ S.M. Nahid, S. Nam, and A.M. van der Zande, "Depolarization Field-Induced Photovoltaic Effect in Graphene/α-In₂Se₃/Graphene Heterostructures," *ACS Nano* **18**(22), 14198–14206 (2024).

¹⁷ H. Wang, S. Wu, Y. Chen, Q. Zhao, J. Zeng, R. Yin, Y. Zheng, C. Liu, S. Zhang, T. Lin, H. Shen, X. Meng, J. Ge, X. Wang, J. Chu, and J. Wang, "Bulk photovoltaic effect in two-dimensional ferroelectric α-In₂Se₃," *Sci. China Inf. Sci.* **68**(2), 122401 (2025).

¹⁸ Z. Lei, J. Chang, Q. Zhao, J. Zhou, Y. Huang, Q. Xiong, and X. Xu, "Ultrafast photocurrent hysteresis in photoferroelectric α-In₂Se₃ diagnosed by terahertz emission spectroscopy," *Sci. Adv.* **11**(7), 1–10 (2025).

¹⁹ M. Küpers, P.M. Konze, A. Meledin, J. Mayer, U. Englert, M. Wuttig, and R. Dronskowski, "Controlled Crystal Growth of Indium Selenide, In₂Se₃, and the Crystal Structures of α-In₂Se₃," *Inorg. Chem.* **57**(18), 11775–11781 (2018).

²⁰ L. Liu, J. Dong, J. Huang, A. Nie, K. Zhai, J. Xiang, B. Wang, F. Wen, C. Mu, Z. Zhao, Y. Gong, Y. Tian, and Z. Liu, "Atomically Resolving Polymorphs and Crystal Structures of In₂Se₃," *Chem. Mater.* **31**(24), 10143–10149 (2019).

²¹ C. Manolikas, "New results on the phase transformations of In₂Se₃," *J. Solid State Chem.* **74**(2), 319–328 (1988).

²² J.Y. Jiping Ye, S.S. Sigeo Soeda, Y.N. Yoshio Nakamura, and O.N. Osamu Nittono, "Crystal Structures and Phase Transformation in In₂Se₃ Compound Semiconductor," *Jpn. J. Appl. Phys.* **37**(8R), 4264 (1998).

²³ G. Han, Z. Chen, J. Drennan, and J. Zou, "Indium Selenides: Structural Characteristics, Synthesis and Their Thermoelectric Performances," *Small* **10**(14), 2747–2765 (2014).

²⁴ K. Kambas, J. Fotsing, E. Hatzikraniotis, and C. Julien, "Characteristics of disorder in defective layered semiconductor α-In₂Se₃," *Phys. Scr.* **37**(3), 397–400 (1988).

²⁵ J. Cui, L. Wang, Z. Du, P. Ying, and Y. Deng, "High thermoelectric performance of a defect in α-In₂Se₃-based solid solution upon substitution of Zn for In," *J. Mater. Chem. C* **3**(35), 9069–9075 (2015).

²⁶ K. Kambas, and J. Spyridelis, "Far infrared optical study of α-In₂Se₃ compound," *Mater. Res. Bull.* **13**(7), 653–660 (1978).

²⁷ H.M. Oh, H. Park, C.D. Kim, Y.S. Kim, K.W. Jang, and W.T. Kim, "Growth and Characterization of α-In₂Se₃ Single Crystals Grown by Using the Chemical Transport Reaction Technique," *J. Korean Phys. Soc.* **43**(2), 312–314 (2003).

²⁸ C. De Blasi, A.V. Drigo, G. Micocci, A. Tepore, and A.M. Mancini, "Preparation and characterization of In₂Se₃ crystals," *J. Cryst. Growth* **94**(2), 455–458 (1989).

²⁹ N.O. Kim, H.G. Kim, H.J. Lim, C. Il Lee, M.S. Jin, C.S. Yoon, and W.T. Kim, "Electrical and optical properties of α - In_2Se_3 single crystals with an indium excess," *J. Korean Phys. Soc.* **38**(4), 405–408 (2001).

³⁰ N.D. Raranskii, V.N. Balazyuk, Z.D. Kovalyuk, N.I. Mel'nik, and V.B. Gevik, "Crystal growth and elastic properties of In_2Se_3 ," *Inorg. Mater.* **47**(11), 1174–1177 (2011).

³¹ Y.I. Zhirko, V.M. Grekhov, and Z.D. Kovalyuk, "Characterization , optical properties and electron (exciton) -phonon interaction in bulk In_2Se_3 crystals and InSe nanocrystals in In 2 Se 3 confinement," *J Nanomed Nanosci* **80**, 148 (2018).

³² T.H. Nguyen, V.Q. Nguyen, A.T. Duong, and S. Cho, "2D semiconducting α - In_2Se_3 single crystals: Growth and huge anisotropy during transport," *J. Alloys Compd.* **810**, 151968 (2019).

³³ G. Micocci, A. Tepore, R. Rella, and P. Siciliano, "Electrical Characterization of In_2Se_3 Single Crystals," *Phys. Status Solidi* **126**(2), 437–442 (1991).

³⁴ C. Julien, M. Eddrief, M. Balkanski, E. Hatzikraniotis, and K. Kambas, "Electrical transport properties of In_2Se_3 ," *Phys. Status Solidi* **88**(2), 687–695 (1985).

³⁵ C. Julien, E. Hatzikraniotis, and K. Kambas, "Electrical transport properties of impurity-doped In_2Se_3 ," *Phys. Status Solidi* **97**(2), 579–585 (1986).

³⁶ C. Julien, and M. Balkanski, "Optical and electrical transport studies in $\text{Li}_{0.1}\text{In}_2\text{Se}_3$," *Mater. Sci. Eng. B* **38**(1–2), 1–8 (1996).

³⁷ Y. Dai, S. Zhao, H. Han, Y. Yan, W. Liu, H. Zhu, L. Li, X. Tang, Y. Li, H. Li, and C. Zhang, "Controlled Growth of Indium Selenides by High-Pressure and High-Temperature Method," *Front. Mater.* **8**(January), 1–7 (2022).

³⁸ C. Tang, Y. Sato, K. Watanabe, T. Tanabe, and Y. Oyama, "Selective crystal growth of indium selenide compounds from saturated solutions grown in a selenium vapor," *Results Mater.* **13**, 100253 (2022).

³⁹ Y. Guan, S. Yoshida, J. Obando-Guevara, S. Mondal, S.H. Lee, H. Pfau, and Z. Mao, "Double-Crucible Vertical Bridgman Technique for Stoichiometry-Controlled Chalcogenide Crystal Growth," *Cryst. Growth Des.*, (2025).

⁴⁰ H.-G. Kim, I. Min, and W. Kim, "Phase transition temperature of the α - In_2Se_3 single crystal," *Solid State Commun.* **64**(5), 819–822 (1987).

⁴¹ H. Okamoto, "In-Se (indium-selenium)," *J. Phase Equilibria Diffus.* **25**(2), 201–201 (2004).

⁴² H. Bergeron, L.M. Guiney, M.E. Beck, C. Zhang, V.K. Sangwan, C.G. Torres-Castanedo, J.T. Gish, R. Rao, D.R. Austin, S. Guo, D. Lam, K. Su, P.T. Brown, N.R. Glavin, B. Maruyama, M.J. Bedzyk, V.P. Dravid, and M.C. Hersam, "Large-area optoelectronic-grade InSe thin films via controlled phase evolution," *Appl. Phys. Rev.* **7**(4), (2020).

⁴³ G. Kremer, A. Mahmoudi, M. Bouaziz, M. Rahimi, F. Bertran, J. Dayen, M.L. Della Rocca, M. Pala, A. Naitabdi, J. Chaste, F. Oehler, and A. Ouerghi, "Mexican hat-like valence band dispersion and quantum confinement in rhombohedral ferroelectric alpha- In_2Se_3 ," *Phys. Rev. B* **112**(15), 155418 (2025).

⁴⁴ H. Ji, A. Reijnders, T. Liang, L.M. Schoop, K.S. Burch, N.P. Ong, and R.J. Cava, “Crystal structure and elementary electronic properties of Bi-stabilized α -In₂Se₃,” Mater. Res. Bull. **48**(7), 2517–2521 (2013).

Supplementary Material

Successful growth of low carrier density α -In₂Se₃ single crystals using Se-flux in a modified Bridgman furnace

Soumi Mondal¹, Sreekant Anil², Saurav Islam¹, Yingdong Guan¹, Sai Venkata Gayathri Ayyagari², Aaron Pearre¹, Sandra Santhosh¹, Nasim Alem², Nitin Samarth¹, Zhiqiang Mao^{1,2a)}

¹Department of Physics, The Pennsylvania State University, University Park, Pennsylvania 16802, USA

²Department of Materials Science and Engineering, The Pennsylvania State University, University Park, PA 16802, USA

^{a)} Author to whom correspondence should be addressed: zim1@psu.edu



Figure S1. Simulated electron diffraction patterns along [2110] zone axis of (a) 3R- α -In₂Se₃ and (b) 2H- α -In₂Se₃. The CIF file used was obtained from CCDC Deposition Number 1855522. The cell parameters for the 2H phase were taken from the supplementary information of the paper: 'Controlled Crystal Growth of Indium Selenide, In₂Se₃, and the Crystal Structures of α -In₂Se₃'¹. The diffraction patterns were simulated using SingleCrystal software

The simulated electron diffraction patterns along the [2110] zone axis for 3R α -In₂Se₃ and 2H α -In₂Se₃ are shown in **Fig. S1a** and **Fig. S1b** respectively. Although the sample adopts the 3R α -In₂Se₃ structure, it contains twin planes. The diffraction pattern in **Fig. S2b** exhibits extra reflections and streaks, which arise from the presence of a twin plane (indicated in **Fig. S2a, c**). Based on the symmetry of the pattern, these twin planes are related by a mirror plane oriented parallel to the c-axis. The ADF-STEM image (**Fig. S2c**) further confirms this, as the atomic arrangement on either side of the white line is mirrored with respect to a plane parallel to the c-axis.

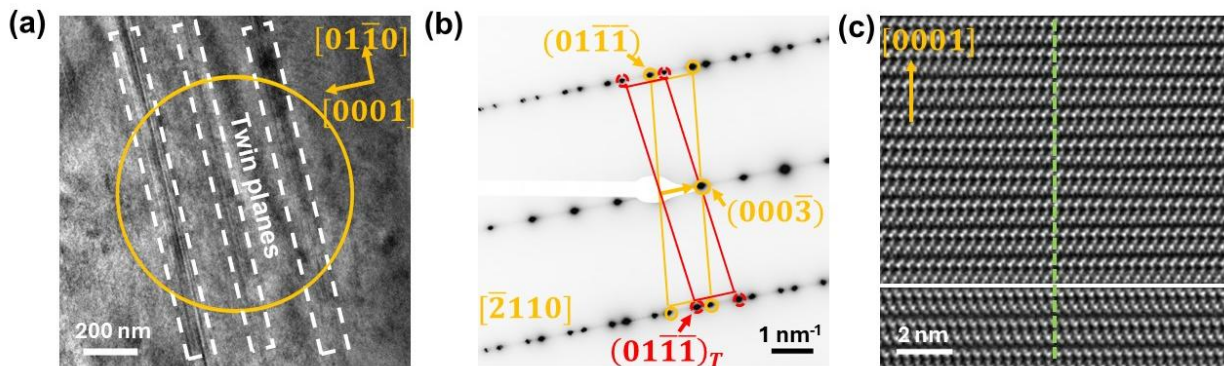


Figure S2. (a) TEM image of 3R- α - In_2Se_3 viewed along the $[\bar{2}110]$ zone axis. (b) Corresponding SAED pattern from the circled region in (a), displaying additional reflections associated with the twin plane. (c) ADF-STEM image in which the twin boundary is clearly visible, indicated by the white line.

References:

¹ M. Küpers, P.M. Konze, A. Meledin, J. Mayer, U. Englert, M. Wuttig, and R. Dronskowski, “Controlled Crystal Growth of Indium Selenide, In_2Se_3 , and the Crystal Structures of α - In_2Se_3 ,” *Inorg. Chem.* **57**(18), 11775–11781 (2018).